JOURNAL OF PROPULSION AND POWER
Vol. 16, No. 1, January–February 2000

Numerical Investigation of Hydrogen Strut Injections into Supersonic Airflows

P. Gerlinger* and D. Brüggemann†
University of Stuttgart, 70550 Stuttgart, Germany

The influence of different injector geometries on the mixing behavior of planar supersonic jets is investigated. Hydrogen is injected in the flow direction through the blunt end of a strut. Different lip thicknesses at the injector end induce different extents of recirculation zones. Additionally, changes are caused within the shock-wave/expansion fan pattern at the injector exit that have an important influence on loss in total pressure. The accuracy of the used numerical scheme is demonstrated for one injector geometry by comparison with experimental data. Based on this configuration, modifications in lip thickness and injection Mach number are investigated numerically and are assessed using several calculated performance parameters. Results show that the chosen lip thickness has a much stronger influence on loss in total pressure than moderate modifications in injector length and height. For the very thin hydrogen jets that were investigated, the mixing efficiency is nearly independent on injector lip thickness.

Introduction

THE understanding of fuel–air mixing and its optimization in supersonic flows is equally important to the development of supersonic combustors and oblique detonation wave engines. In both cases the available time to achieve mixing is on the order of a millisecond. In addition to good mixing, thrust losses must be identified to work on their minimization. There are different kinds of thrust losses associated with the fuel injection of a real combustor: losses due to incomplete mixing, viscous effects, and shock waves.[1] The degree of irreversible entropy gain caused by these processes directly follows from the way that fuel is injected. Irreversibilities are caused, e.g., by the mixing itself as well as by shock waves induced at the injector. Shock waves are unavoidable in supersonic flows, but often can be employed to enhance the mixing process.[2–4] Thus, concepts for an improved mixing by a generation of shock waves or vorticity results in thrust losses. Detailed studies of thrust losses of hypersonic engines are given in Refs. 1 and 5.

Because of their particular properties concerning mixing efficiency and thrust losses, different kinds of injectors may be used at different flight Mach numbers.[6] Various kinds of injection concepts have been investigated in the literature to reduce separation zones and accelerate penetration into the freestream.[7–10] Transverse fuel injections in most cases cause a strong blockage of the main flow,[11] which, associated with irreversibilities of the resulting shock waves, lead to strong thrust losses.[5] On the other hand, good near-field mixing is possible. Parallel fuel injection may be achieved without the induction of shock waves, but at the cost of unfavorable mixing, and, therefore, longer combustors. However, Papamoschou[12] has clearly shown in an analytical study that viscous dissipation associated with strong velocity differences also causes large losses in total pressure. These losses are connected to a reduced thrust and may be comparable with losses due to transverse fuel injection for convective Mach numbers on the order of or more than 1.

In contrast to the more fundamental studies in Ref. 12, the purpose of this paper is to investigate axial hydrogen mixing for a real strut injector used in a subscale mixing and combustion chamber. Struts offer the possibility of injecting hydrogen directly into the core of a supersonic flow.[13] On the other hand, the strut is exposed to the main flow and subsequent losses must be evaluated. A planar thin hydrogen jet of 0.6-mm thickness is injected into a cold Mach 2 surrounding airflow. This injector suffers from finite wall thicknesses at the nozzle end, and, in case of combustion, from problems with heating. Based on an experimentally realized configuration, the influence of different injector geometries is simulated numerically. The detail problem of practically unavoidable injector lip thicknesses and their influence on flow structure, turbulence production, and loss in total pressure is investigated. An additional point is an optimization of the strut's shape concerning losses in total pressure. Calculations are performed for cold gases with matched, under- and overexpanded hydrogen jets.

Governing Equations

The investigation of high-speed turbulent mixing requires the solution of the full Navier–Stokes and species transport equations that are given in two-dimensional conservative form by

$$\frac{\partial \boldsymbol{Q}}{\partial t} + \frac{\partial (\boldsymbol{F} - \boldsymbol{F}_v)}{\partial x} + \frac{\partial (\boldsymbol{G} - \boldsymbol{G}_v)}{\partial y} = 0 \tag{1}$$

where the conservative variable vector is

$$\boldsymbol{Q} = [\rho, \rho u, \rho v, \rho E, \rho q, \rho \omega, \rho Y_i]^t \tag{2}$$

$\boldsymbol{F}$ and $\boldsymbol{G}$ are inviscid; and $\boldsymbol{F}_v$ and $\boldsymbol{G}_v$ are the viscous fluxes in the x and y direction, respectively. In Eq. (2), ρ is the density, u and v are the velocity components in the x and y direction, E is the total specific energy, the turbulence variables are $q = \sqrt{k}$ (k is the turbulent kinetic energy) and $\omega = \varepsilon / k$ (ε is the dissipation rate of k), and Y_i are the species mass fractions. The following calculations are performed with three different species: N_2, O_2, and H_2. For turbulence closure, a low-Reynolds-number two-equation q-ω turbulence model is employed.[14,15] This turbulence model is well suited for supersonic flows. Turbulent Prandtl and Schmidt numbers of 0.9 are assumed to calculate turbulent contributions to heat conductivity and diffusivity.

The unsteady form of the governing equations is integrated in time using the implicit turbulent all speed combustion multigrid (TASCOM) finite volume solver[16,17] based on an lower–upper symmetric Gauss–Seidel (LU–SGS) algorithm.[18,19] Multigrid is used as convergence acceleration for all conservation equations.[20,21] Steady states are reached in less than 7000 iterations. The residuals of both fluid and turbulence variables reached machine accuracy of the employed NEC–SX4. The numerical multiblock code has been extensively tested and compared with experimental data.

Received 10 June 1998; revision received 25 January 1999; accepted for publication 4 February 1999.

*Research Scientist, Institut für Thermodynamik der Luft- und Raumfahrt, Pfaffenwaldring 31; peter.gerlinger@itlr.uni-stuttgart.de. Member AIAA.

†Professor, Institut für Thermodynamik der Luft- und Raumfahrt, Pfaffenwaldring 31; dieter-brueggemann@itlr.uni-stuttgart.de.

Grid and Inflow Conditions

The numerical studies are based on a geometrical configuration that is investigated experimentally at the Institut für Thermodynamik der Luft- und Raumfahrt (ITLR), University of Stuttgart, supersonic test facility. Figure 1 shows the rectangular Mach 2 convergent–divergent nozzle section. After expansion, the duct has a constant cross section of 35.4 × 40 mm (channel height × depth). The chosen inflow conditions produce a freestream Reynolds number of 4.96×10^7 per meter. Computations start at the nozzle throat ($x = 0$ mm) with sonic conditions. The channel height at the nozzle throat is 20.12 mm. Because of the symmetric geometry, calculations are performed for only the upper part of the channel. A fully turbulent boundary layer is assumed at the inlet for all calculations. Because the boundary-layer thickness is not known from the experiment, a value of $\delta = 0.4$ mm has been assumed. A turbulent inflow boundary layer is important to prevent the q-ω turbulence model from going through transition. Pure hydrogen is injected through the blunt end of a strut positioned on the channel centerline. A second nozzle inside the strut is designed for an injection Mach number of about 2.3. In case of unmatched pressure, an expansion fan or an oblique shock wave occurs directly at the nozzle exit or inside the nozzle. To simulate these effects, the computation includes the divergent part of the injector geometry inside the strut. The inflow conditions for the hydrogen injector are sonic conditions at the injector nozzle throat located at $x = 172$ mm.

A three-block grid with 472 × 32, 432 × 56, and 672 × 96 volumes is used for a simulated channel length of 500 mm. The nozzle inside the strut is simulated with 40 volumes in a streamwise direction. An enlargement of the computational grid near the end of the strut (only the upper symmetric part) is given in Fig. 2. The computational grid is strongly refined near solid walls and in the mixing zone downstream of the injector, leading to highly stretched grids in these regions. All y^+ values for near-wall cell centers should be smaller than 1, which is a requirement for accurate use of the chosen low-Reynolds-number turbulence model. At stationary conditions all y^+ values at the channel walls are smaller than 0.5. At the outer surface of the strut the maximum y^+ values are 1.65 at the tip and 1.2 at the end of the strut, where the boundary layer is accelerated with the formation of an expansion fan. Between these points, as well as at the blunt end of the strut and inside the hydrogen nozzle, all y^+ values are considerably smaller than 1. To satisfy this constraint, cell heights smaller than 0.5×10^{-6} m had to be chosen. The high velocities within the hydrogen injector particularly required such small wall distances. Further grid refinements had no influence on all investigated performance parameters. The sonic inflow conditions for the main airstream and the injected hydrogen are given in Table 1. The corresponding jet-to-freestream momentum flux ratio[22] $m_r = (\rho u^2)_j/(\rho u^2)_\infty$ is 0.87. The mass flow rates of air and hydrogen are 0.74 kg/s and 2.4 g/s, respectively. These flow rates result in an understoichiometric ratio of 0.105.

Table 1 Inflow conditions for the main airstream and the hydrogen jet

Parameter	Main airstream	Hydrogen jet
p, bar	2.05	1.95
T, K	240	260
Ma	1	1
Y_{H_2}	0	1
Y_{N_2}	0.7664	0
Y_{O_2}	0.2336	0

Results and Discussion

The computational effort is divided into two parts. The first one deals with the demonstration and validation of the numerical scheme by comparison with experimental data for a basic injector configuration. The second part investigates and quantifies influences resulting from changes in basic strut geometry.

Comparison with Experiment

The experiment is based on a Mach 2.3 hydrogen injector with a lip height of $h = 0.7$ mm at the end of the strut. This strut is the basis for later modifications and has a length of $L = 80$ mm and a height of $H = 6$ mm, respectively. Geometry and inflow conditions given in Table 1 result in slightly mismatched static pressure at the injector exit. Figure 3 shows a comparison of flow structure between a schlieren photograph of the experiment and a calculated pressure distribution. The shock waves and expansion fans along the strut agree very well. In the schlieren photograph a slight unsymmetry may be observed in the shock reflections at the upper and lower strut surface. The outer edges at the end of the strut cause expansion fans that are directly followed by shock waves. Figures 4 and 5 compare measured and calculated molar fraction profiles of H_2 and N_2 at four different locations. The profiles are given at $x =$ 178, 225, 275, and 325 mm. Although there are some differences in the outer parts of the profiles, the calculated decay of maximum values at the channel centerline agrees quite well with experimental data. A discrepancy is the approximately 20% smaller mixing-layer thickness obtained by the calculation. Figure 6 shows a comparison between measured and calculated static pressure profiles along the upper channel wall. The comparison is given for the first 300 mm where experimental data are available. While the agreement between experiment and computation is fairly good up to the end of the strut, differences are found farther downstream. They are mainly caused by slightly shifted locations of shock waves and expansion fans traveling downstream. However, the overall agreement between computation and experiment is quite good, taking into account the complexity of the problem. The validation was a presumption for using the TASCOM solver to investigate the influence of geometric modifications. Moreover, to confirm the conservative nature of the solver, integrated mass flow rates of air and hydrogen have been calculated for all investigated cases. The calculations conserved mass to within 1%. Further details about the ITLR supersonic test facility as well as the Raman measurement technique have been described in Refs. 23 and 24.

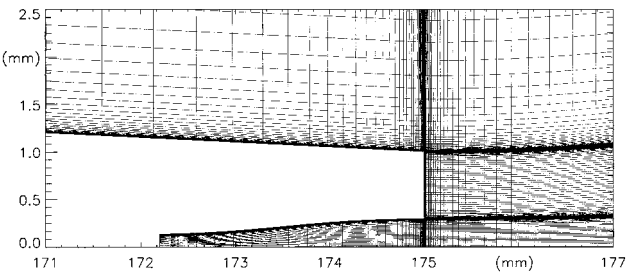

Fig. 2 Enlargement of the computational grid at the hydrogen injector exit.

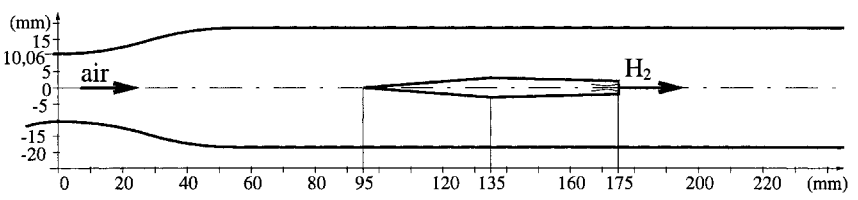

Fig. 1 Channel geometry (mm).

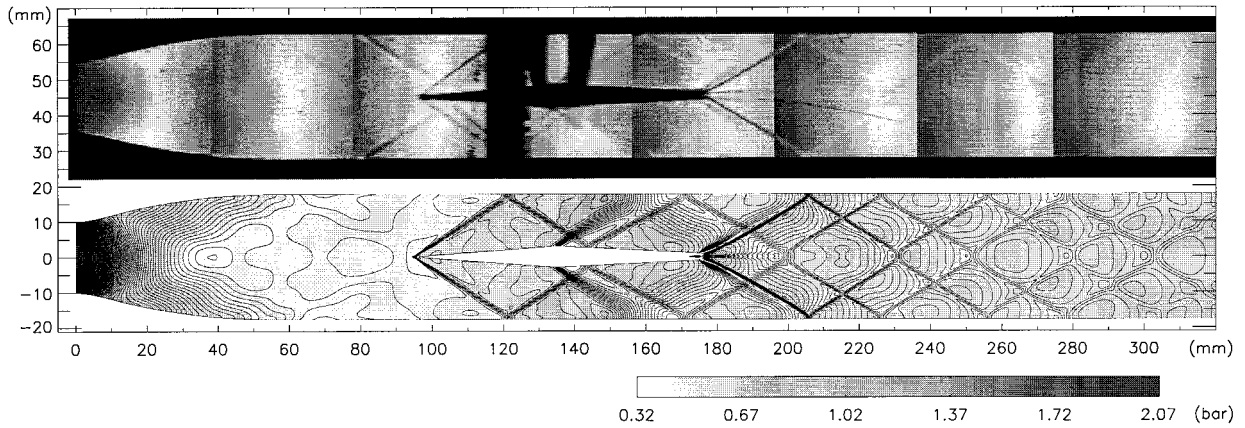

Fig. 3 Schlieren photograph and calculated pressure distribution.

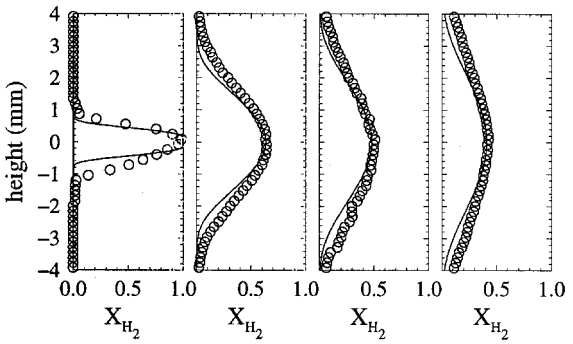

Fig. 4 Measured (∘) and calculated (——) H_2 profiles.

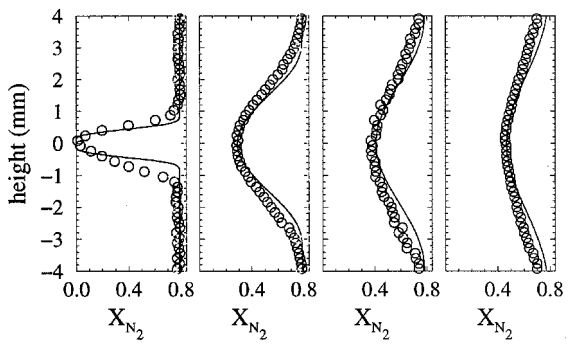

Fig. 5 Measured (∘) and calculated (——) N_2 profiles.

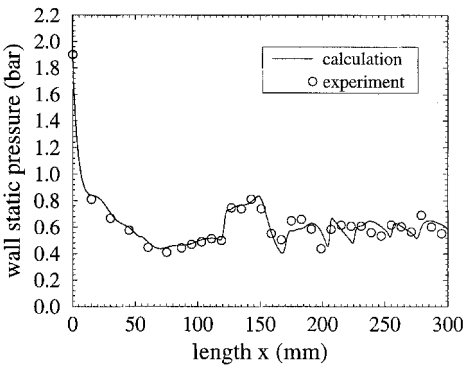

Fig. 6 Measured (∘) and calculated (——) wall static pressures.

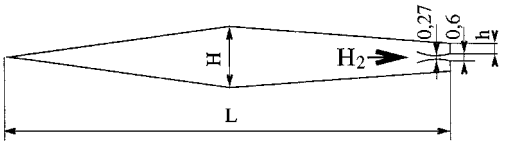

Fig. 7 Geometry (mm) of the investigated struts for hydrogen injection.

Modifications in Strut Geometry

While most analytical investigations on hydrogen mixing assume splitter plates of negligible thickness,[25–29] real injectors exhibit lip thicknesses that are often specified by manufacturing restraints. In case of combustion, thermal loads may cause additional problems. Bluff bodies are also often used for flame stabilization.[30] Figure 7 shows a strut configuration for which the lip thickness h, the length L, and the height H are varied, keeping the nozzle geometry constant. The height of the nozzle throat is 0.27 mm and the jet height at the nozzle exit 0.6 mm. The comparison with experimental data described in the last section was performed for the basic configuration with $h = 0.7$ mm, $H = 6$ mm, and $L = 80$ mm. It is obvious that a reduction in h reduces the loss in total pressure. On the other hand, negligible lip thicknesses may not be applied in case of combustion due to severe cooling problems of the lip. Experimental investigations found a lip thickness of $h = 0.7$ mm to be suited for hot long time runs without damaging the strut. The following parameter study investigates quantatively the influence of different strut modifications on mixing efficiency, mixing-layer thickness, and loss in total pressure. Only one parameter (h, H, or L) is always changed at a time, keeping all remaining geometrical values in accordance with the basic configuration. Hydrogen and air inflow conditions always remain unchanged.

An important parameter to evaluate compressibility effects in shear flows is the convective Mach number. Because of the strong differences in the speed of sound and the resulting strong velocity differences between the hydrogen jet and surrounding air, similar effects such as for pure shear flows occur in the present case. If a convective Mach number is calculated with flow conditions at the injector exit, a relatively high supersonic value of about 1.23 is obtained for the present configurations. The air main stream velocity ($u_{\text{air}} = 500$ m/s) and the centerline velocity of the hydrogen jet ($u_{H_2} = 2030$ m/s) at the injector exit cross section ($x = 175$ mm) are used for its calculation:

$$M_c(x) = \frac{\Delta U}{a_{\infty,\text{air}} + a_{\infty,H_2}} \tag{3}$$

ΔU is the velocity difference between both streams, and $a_{\infty,\text{air}}$ and a_{∞,H_2} are the corresponding speeds of sound. While for pure shear flows the convective Mach number is maintained in a streamwise

direction in the present case, its decay to zero strongly depends on the thickness of the jet. Thus, at least in the first part downstream of the injector, where large values for the convective Mach number are obtained, similar effects such as that for pure shear flows may occur. The most important effect is a decrease in the growth rate of compressible mixing layers at high convective Mach numbers[25,26] in comparison with incompressible ones. For the investigated hydrogen, air-mixing influences due to high-density ratios between both streams additionally may have an effect on the spreading rate.[29] However, due to the thinness of the injected hydrogen jet (0.6 mm), normal velocity gradients decay to less than 1% of their initial value over a length of 80 mm only, thus limiting compressibility effects to the region directly downstream of the injector.

Influence of Injector Lip Thickness

Numerical calculations are performed for five different lip thicknesses $h = 0.1$, 0.4, 0.7, 1.2, and 1.7 mm, whereas the length and height of the strut remain constant. These cases represent underexpanded, matched, and overexpanded hydrogen injections. With the increase in lip thickness, the angle from the end to the middle of the strut reduces from 2.86 to 1.43 deg. Small recirculation zones appear at the blunt ends of the struts formed by two vortices rotating in opposite directions. Their extent is about 0.7, 2, and 4 mm for the 0.1, 0.7, and 1.7 mm lip height, respectively.

Figure 8 shows calculated pressure contours for three out of five cases with lip thicknesses h of 0.1, 0.7, and 1.7 mm. With increasing step height the change in the outer airflow direction increases, causing stronger expansion fans and shock waves. This results in decreasing pressure levels (0.5, 0.36, and 0.28 bar) in the recirculation zone downstream of the lip. While in the first case an oblique shock wave is formed at the nozzle exit, the pressure is nearly matched in the second case, and, an expansion fan occurs in the third calculation.

To investigate the influence of unmatched static pressure at the hydrogen nozzle exit, a second series of calculations is performed. While the inflow conditions, the height of the throat, and the height of the strut's blunt end remain constant, different injector exit heights, and, subsequently, varied lip thicknesses, result in matched static pressures and different exit Mach numbers. However, the differences between the cases with matched and unmatched static pressures are hardly visible in all performance parameters. For the chosen strut it seems to be less important if the injected hydrogen jet is slightly over- or underexpanded if the injection total pressure is kept constant. Losses or gains due to these effects are small in comparison with other sources. Thus, unmatched pressure for the hydrogen injection is no source for differences in performance parameters discussed later.

Figure 9 shows contours of q ($q = \sqrt{k}, k =$ turbulent kinetic energy) for the same three lip thicknesses. Maximum values increase from 220 to 310 m/s with increasing lip height caused by larger extents of the recirculation zone and increasing shock strength. This increase is independent of matched or unmatched static pressure at the hydrogen nozzle exit (calculations with matched static pressure produce similar results). The production of turbulent kinetic energy within the recirculation zones is negligible in comparison with the production in the following shock wave or in the shear layer of the hydrogen jet. However, there also are high values of ω ($\omega = \varepsilon / k$, $\varepsilon =$ dissipation rate of k) in the shear layer. An important parameter for the mixing process is the turbulent diffusivity that is obtained from eddy viscosity ($\mu_t \sim q^2/\omega$) under the assumption of a constant turbulent Schmidt number. Figure 10 shows contours of q, $\log(\omega/\omega_\infty)$, and $\mu_t/\mu_{l,\mathrm{ref}}$ for the basic strut geometry ($h = 0.7$ mm), where ω_∞ is the freestream values in front of the strut and $\mu_{l,\mathrm{ref}}$ is a reference laminar viscosity. The shock wave induced at the tip of the strut is reflected at the upper wall and hits the strut again at about $x = 140$ mm, resulting in slightly increased values of q. Strongly increased values of μ_t are found for all cases above the strut between $x = 140$ and 175 mm. This region of high-eddy viscosity is shifted farther upward with increasing lip height. Additionally, μ_t is increased by stronger shock waves downstream of the recirculation zone. Thus, differences in eddy viscosity distribution caused by larger lip heights are mainly found in the outer part of the flowfield ($y > 1$ mm), whereas the distributions near the channel centerlines are quite similar. This may be also seen from Fig. 11 where transverse profiles of q are plotted at $x = 195$ mm. Only small differences are found near the channel centerline, whereas the profiles significantly differ with transition to freestream turbulence. It is also important to note that the main positive production of q and ω is in the rapidly decaying shear layer between hydrogen jet and airflow. Already, 5 mm downstream of the nozzle, values are again

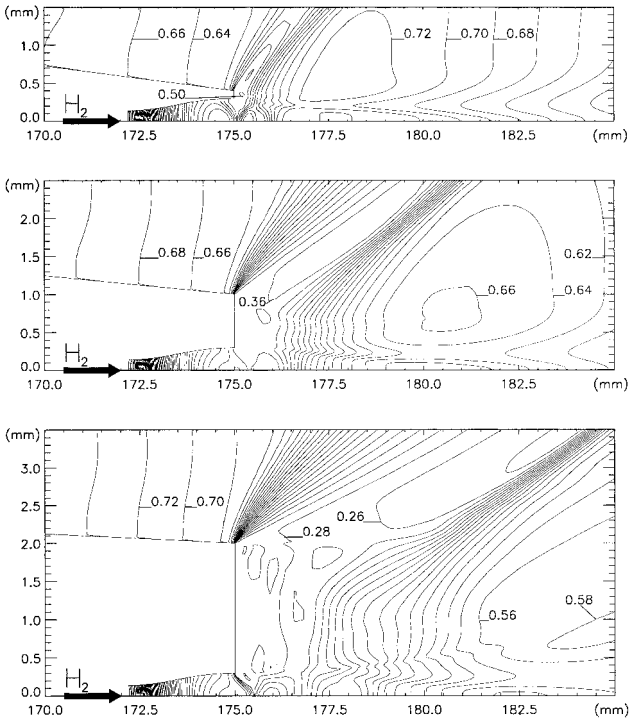

Fig. 8 Pressure contours (bar) at the injector exit with $h = 0.1$, 0.7, and 1.7 mm ($\Delta = 0.02$ bar).

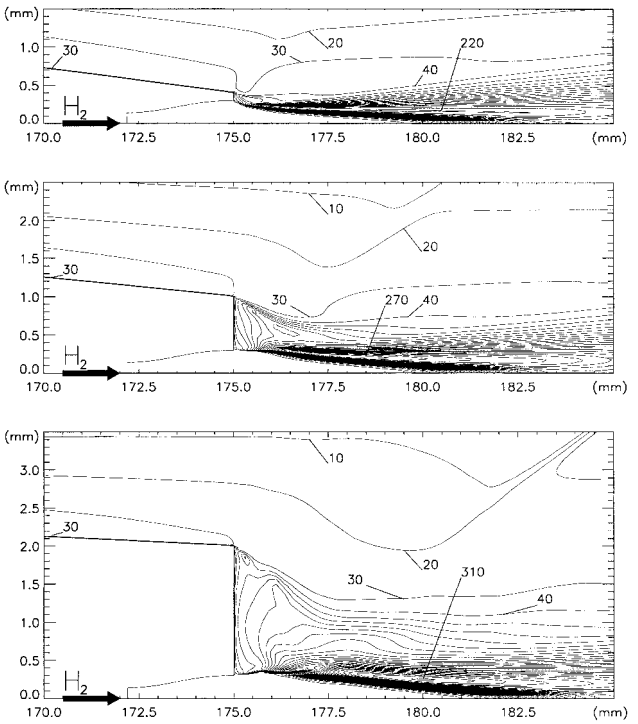

Fig. 9 Contours of q (m/s) at the injector exit with $h = 0.1$, 0.7, and 1.7 mm ($\Delta = 10$ m/s).

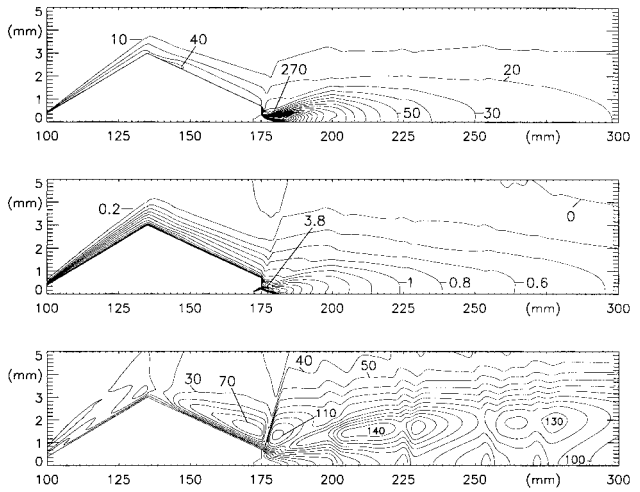

Fig. 10 Contours of q (m/s, Δ = 10 m/s); $\log(\omega/\omega_\infty)$ (Δ = 0.2); and $\mu_t/\mu_{t,\mathrm{ref}}$ (Δ = 10) for the strut with h = 0.7 mm.

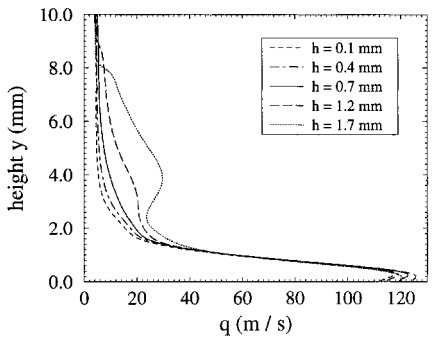

Fig. 11 Profiles of q (m/s) at x = 195 mm.

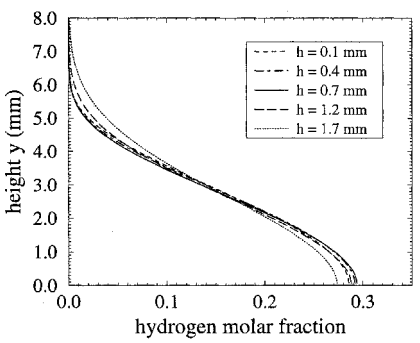

Fig. 12 Hydrogen profiles at the channel end at x = 500 mm.

decreasing. However, the different dissipation rates of q and ω only cause a moderate reduction in eddy viscosity, and significant diffusivities are still found far downstream of the strut where convective Mach number and normal velocity gradients are zero.

Mixing

Figure 12 shows profiles of hydrogen molar fractions at x = 500 mm. Despite the similarity of the profiles, a clear trend may be seen from this figure. With increasing lip thickness the profiles broaden in normal direction. This is usually associated with a decrease in maximum values at the channel centerline. Only small differences are obtained for the three smallest lip heights.

To investigate the growth of the mixing-layer more accurately a mixing-layer thickness is introduced. The mixing-layer thickness is defined as the distance between the transverse locations of the symmetric profile where the molar fractions of hydrogen are 0.05. In Fig. 13 these values are plotted vs the length of the channel. Note that injection takes place at x = 175 mm. The maximum difference in mixing-layer thickness at the channel end is about 10%. The profiles in Fig. 13 strongly differ from the smooth distributions obtained for shear flows over a splitter plate.[25] This is due to two facts. First, directly downstream of the injector lip, a hydrogen-rich recirculation zone is obtained. Therefore, the mixing-layer thickness directly at the injector exit amounts to about the height of the strut's blunt end (0.6 mm + 2h). Because of the expansion fans formed at the outer edge of the strut, the mixing layer is first contracted, leading to a decrease. The minimum values increase and slightly shift farther downstream with increasing lip height. The second difference to a splitter plate is the wave-like increase in mixing-layer thickness over the channel length. This is due to shock waves traveling downstream and being reflected at the channel walls. It is interesting that all five cases result in similar values and gradients downstream of the recirculation zone between x = 190 and 200 mm. The first strong increase up to a mixing-layer thickness of about 5 mm is caused by the high turbulent diffusivities downstream and above the struts blunt end (see Fig. 10). This is quite similar for all investigated cases. When reaching the edge of the high-diffusivity region, increases in the mixing-layer thickness slows down, leading to a less-steep increase farther downstream. The differences in the curves plotted in Fig. 13 are mainly caused by different extents of regions with increased diffusivity extending into the main stream.

While up to now the mixing-layer thickness was the critical parameter, the mixing efficiency will now be studied. The mixing efficiency is defined as the fraction of hydrogen mass flux that could react due to available oxygen (if complete reaction took place), and is calculated by[22]

$$\eta_{\mathrm{mix}} = \frac{\int_A \rho u Y_{\mathrm{H}_2,r}\,\mathrm{d}A}{\dot{m}_{\mathrm{H}_2}} \tag{4}$$

where $Y_{\mathrm{H}_2,r}$ is the hydrogen fraction that could react, A is the channel cross section, and $\dot{m}_{\mathrm{H}_2}$ is the injected hydrogen mass flux. If the mixing efficiency adds up to 1, all available hydrogen could react because oxygen is avaiable at least at a stoichiometric rate. Figure 14 shows the mixing efficiency plotted over the channel length. Two conclusions may be deduced from this plot. First, while there is some

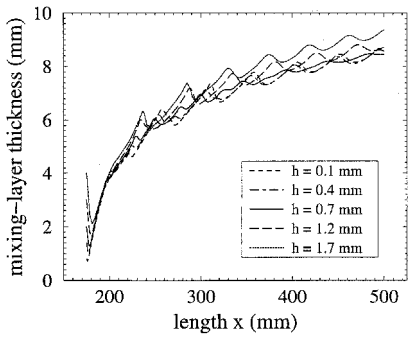

Fig. 13 Mixing-layer thickness based on molar hydrogen fractions.

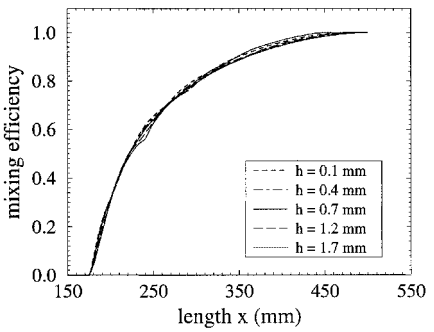

Fig. 14 Mixing efficiency.

Table 2 Loss in total pressure (%) until reaching a mixing efficiency of 1[a]

Dimension	h = 0.1 mm	h = 0.4 mm	h = 0.7 mm	h = 1.2 mm	h = 1.7 mm
H = 6, L = 80	14.98	15.49	16.09	16.91	17.94
H = 4, L = 80	14.79	——	15.62	——	17.77
H = 8, L = 80	15.22	——	16.32	——	18.35
H = 6, L = 60	15.52	——	15.59	——	17.50

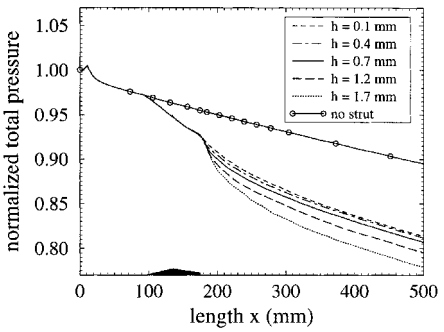

Fig. 15 Normalized mass-flow-averaged total pressure.

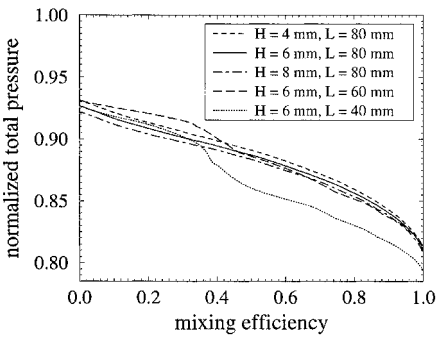

Fig. 16 Normalized mass-flow-averaged total pressure vs mixing efficiency for h = 0.7 mm and different strut geometries.

influence of the injector lip thickness on the mixing-layer thickness, there is nearly no influence on the mixing efficiency. Second, complete mixing is achieved for all cases 300 mm downstream of the injector. The reason for the negligible differences of the five cases in mixing efficiency is the smallness of the hydrogen jet. The decrease of maximum hydrogen fraction near the channel centerline is the critical parameter for the mixing efficiency. In the outer regions of the profiles, all hydrogen may react due to available oxygen. The decrease of hydrogen maximum values basically depends on the turbulence intensity along the channel centerline. The turbulence levels on the other hand are only slightly affected by the lip thickness. Most important is the production of q and ω in the shear layer of the hydrogen jet that causes high diffusivities near the channel centerline that are quite similar for all investigated cases.

Losses

In addition to the mixing performance, losses due to mixing are a crucial factor for the assessment of any injector. The different shock patterns caused by various injector geometries result in different losses in total pressure. Figure 15 shows the normalized total pressures that depend on the streamwise direction. The normalized mass flux-averaged total pressure is calculated for every channel cross section by

$$\bar{p}_t = \frac{1}{\dot{m}} \int_A p_t \rho u \, \mathrm{d}A \tag{5}$$

where p_t is the total pressure determined from the Mach number and static pressure. The employed central difference scheme allows small pressure oscillations near shock waves that may also be observed in total pressure profiles. Independent of under- or over-expanded injection, Fig. 15 clearly shows that an increase in lip thickness causes stronger losses in total pressure due to stronger shock waves. The location of the strut is plotted symbolically on the x axis. As can also be seen from Fig. 15, most of the losses due to higher lip thicknesses occur directly at the injector. A second, rapidly decreasing contribution are losses due to shock waves traveling downstream by wall reflections. Because of the weakening of the shock waves the slopes of all curves approach each other, and, in case of complete mixing, become similar to that of the channel without strut. Away from the injector, the mixing itself as well as the increase in boundary-layer thickness become dominant contributions to loss in total pressure. The losses from the beginning of the strut until reaching a mixing efficiency of 1 are summarized in the first line of Table 2. The difference between the cases with 0.1 and 1.7 mm lip thicknesses is about 17%. The strong contributions of shock waves and increase in boundary-layer thickness also emphasize the necessity to keep combustor lengths short.

Modification of Strut Length and Height

Next, the influence of the shape of the strut is investigated. The greatest disadvantages of the strut concept are losses due to its boundary layers and losses from shock waves caused by the strut. While a short strut reduces the first kind of loss, the second one is increased (for the same strut height). In case of combustion the injected hydrogen is used, as coolant heat losses in the boundary layer may be recovered by hydrogen heating. Figure 16 shows the normalized total pressure vs the mixing efficiency for a lip thickness of 0.7 mm and different strut geometries. With the exception of the shortest strut (L =40 mm), the differences are very small until a mixing efficiency of 1 is reached. The high losses in the last case result from boundary-layer separation at the upper wall. The shock wave caused at the tip of the strut causes this separation after reflection at the strut. The gains of shorter strut lengths are nearly identical to losses caused by stronger shock waves. Results for other lip heights are given in lines 2–4 of Table 2. As long as the wedge angle at the tip of the strut is small enough to avoid boundary-layer separation, moderate changes in the height and length of the strut have a much smaller influence than modifications in lip thickness.

Conclusions

Numerical investigations on the mixing of thin supersonic hydrogen jets in cold supersonic airflows were performed. A comparison with experimental data demonstrated the accuracy and applicability of the employed numerical scheme, turbulence model, and computational grid. Variations in strut geometry have demonstrated several effects:

1) The mixing-layer thickness is shifted to higher values with increasing lip height due to increased diffusivities caused at the struts outer wall and stronger shock waves.

2) The increase in mixing-layer thickness has no significant influence on the mixing efficiency for the investigated thin jets.

3) An increase in a lip height of 1.6 mm resulted in about a 17% larger loss in total pressure.

4) Because of the rapid decay of velocity gradients in the normal direction (for small jets), compressibility effects are important only directly at the injector.

5) Only insignificant differences in mixing efficiency or loss in total pressure are caused by slightly unmatched injector nozzle geometries for the same injection total pressure.

6) The choice of length and height of the strut only has a minor influence on loss in total pressure compared with the lip thickness as long as boundary-layer separation is avoided.

Acknowledgments

The authors wish to thank the Deutsche Forschungsgemeinschaft for the financial support of this work within the Collaborative Research Center SFB 259 at the University of Stuttgart. The authors also thank P. Kasal and J. Boltz for the use of experimental results.

References

[1]Riggins, D. W., McClinton, C. R., and Vitt, P. H., "Thrust Losses in Hypersonic Engines Part 1: Methodology," *Journal of Propulsion and Power*, Vol. 13, No. 2, 1997, pp. 281–287.

[2]Menon, S., "Shock-Wave Induced Mixing Enhancement in Scramjet Combustors," AIAA Paper 89-0104, Jan. 1989.

[3]Guirguis, R. H., Grinstein, F. F., Young, T. R., Oran, E. S., Kailasanath, K., and Boris, J. P., "Mixing Enhancement in Supersonic Mixing Layers," AIAA Paper 87-0373, Jan. 1987.

[4]Fernando, E. M., and Menon, S., "Mixing Enhancement in Compressible Mixing Layers: An Experimental Study," *AIAA Journal*, Vol. 31, No. 2, 1993, pp. 278–285.

[5]Riggins, D. W., "Thrust Losses in Hypersonic Engines, Part 2: Applications," *Journal of Propulsion and Power*, Vol. 13, No. 2, 1997, pp. 288–295.

[6]Donohue, J. M., McDaniels, J. C., Jr., and Haj-Hariri, H., "Experimental and Numerical Study of Swept Ramp Injection into a Supersonic Flowfield," *AIAA Journal*, Vol. 32, No. 9, 1994, pp. 1860–1867.

[7]Barber, M. J., Schetz, J. A., and Roe, L. A., "Normal, Sonic Helium Injection Through a Wedge-Shaped Orifice into Supersonic Flow," *Journal of Propulsion and Power*, Vol. 13, No. 2, 1997, pp. 257–263.

[8]Bogdanoff, D. W., "Advanced Injection and Mixing Techniques for Scramjet Combustion," *Journal of Propulsion and Power*, Vol. 10, No. 2, 1994, pp. 183–190.

[9]Hyde, C. R., Smith, B. R., Schetz, J. A., and Walker, D. A., "Turbulence Measurements for Heated Gas Slot Injection in Supersonic Flow," *AIAA Journal*, Vol. 28, No. 9, 1990, pp. 1605–1614.

[10]Baurle, R. A., Fuller, R. P., White, J. A., Chen, T. H., Gruber, M. R., and Nejad, A. S., "An Investigation of Advanced Fuel Injection Schemes for Scramjet Combustion," AIAA Paper 98-0937, Jan. 1998.

[11]Belanger, J., and Hornung, H. G., "Transverse Jet Mixing and Combustion Experiments in Hypervelocity Flows," *Journal of Propulsion and Power*, Vol. 12, No. 1, 1996, pp. 186–192.

[12]Papamoschou, D., "Thrust Loss Due to Supersonic Mixing," *Journal of Propulsion and Power*, Vol. 10, No. 6, 1994, pp. 804–809.

[13]Tomioka, S., Murakami, A., Kudo, K., and Mitani, T., "Combustion Tests of a Staged Supersonic Combustor with a Strut," AIAA Paper 98-3273, July 1998.

[14]Coakley, T. J., and Huang, P. G., "Turbulence Modeling for High Speed Flows," AIAA Paper 92-0436, Jan. 1992.

[15]Gerlinger, P., Algermissen, J., and Brüggemann, "Numerical Simulation of Mixing for Turbulent Slot Injection," *AIAA Journal*, Vol. 34, No. 1, 1996, pp. 73–78.

[16]Gerlinger, P., and Algermissen, J., "Numerical Calculation of Supersonic Combustion Problems Using an Implicit LU-SGS Scheme and k-ε/q-ω Turbulence Closure," AIAA Paper 93-5021, Nov. 1993.

[17]Gerlinger, P., Algermissen, J., and Brüggemann, D., "Matrix Dissipation for Central Difference Schemes with Combustion," *AIAA Journal*, Vol. 33, No. 10, 1995, pp. 1865–1870.

[18]Shuen, J. S., "Upwind Differencing and LU Factorization for Chemical Non-Equilibrium Navier–Stokes Equations," *Journal of Computational Physics*, Vol. 99, No. 2, 1992, pp. 233–250.

[19]Yoon, S., and Jameson, A., "An LU-SSOR Scheme for the Euler and Navier–Stokes Equations," AIAA Paper 87-0600, Jan. 1987.

[20]Gerlinger, P., and Brüggemann, D., "Multigrid Convergence Acceleration for Turbulent Supersonic Flows," *International Journal for Numerical Methods in Fluids*, Vol. 24, June 1997, pp. 1019–1035.

[21]Gerlinger, P., Stoll, P., and Brüggemann, D., "An Implicit Multigrid Method for the Simulation of Chemically Reacting Flows," *Journal of Computational Physics*, Vol. 146, No. 1, 1998, pp. 322–345.

[22]Fuller, R. P., Wu, P.-K., Nejad, A. S., and Schetz, J. A., "Fuel-Vortex Interactions for Enhanced Mixing in Supersonic Flow," AIAA Paper 96-2661, July 1996.

[23]Brellochs, F., Fertig, M., Algermissen, J., and Brüggemann, D., "Optical Measurements of Hydrogen Mixing in Supersonic Airflows," *Combustion in Supersonic Flows*, edited by M. Champion and B. Deshaies, Kluwer Academic, Norwell, MA, 1997, pp. 71–97.

[24]Kasal, P., Boltz, J., Gerlinger, P., and Brüggemann, D., "Raman Measurements of Supersonic Hydrogen/Air Mixing," *Laser Applications to Chemical and Environmental Analysis, OSA Technical Digest*, Vol. 3, March 1998, pp. 95–97.

[25]Papamoschou, D., "Analysis of Partially Mixed Supersonic Injector," *Journal of Propulsion and Power*, Vol. 12, No. 4, 1996, pp. 736–741.

[26]Oh, C., and Loth, E., "A Numerical Investigation of Supersonic Turbulent Shear Layers: Compressibility Effects," AIAA Paper 94-2244, June 1994.

[27]Groebel, S. G., and Dutton, J. C., "Experimental Study of Compressible Turbulent Mixing Layers," *AIAA Journal*, Vol. 29, No. 4, 1991, pp. 538–546.

[28]Papamoschou, D., and Roshko, A., "The Compressible Turbulent Shear Layer: An Experimental Study," *Journal of Fluid Mechanics*, Vol. 197, Dec. 1988, pp. 453–477.

[29]Kozusko, F., Lasseigne, D. G., Grosch, C. E., and Jackson, T. L., "The Stability of Compressible Mixing Layers in Binary Gases," NASA CR-198334, Inst. for Computer Applications in Science and Engineering, Rept. 96-33, NASA Langley Research Center, Hampton, VA, 1996.

[30]Huh, H., and Discroll, J. F., "Measured Effects of Shock Waves on Supersonic Hydrogen-Air Flames," AIAA Paper 96-3035, July 1996.